Multiwalled Carbon Nanotubes Display Microtubule Biomimetic Properties *in Vivo*, Enhancing Microtubule Assembly and Stabilization

Lidia Rodriguez-Fernandez,[†] Rafael Valiente,[‡,*] Jesús Gonzalez,[§] Juan C. Villegas,[⊥] and Mónica L. Fanarraga[∥,*]

[†]SERMET-SCTI, [‡]Departamento de Física Aplicada, Facultad de Ciencias, and [§]MALTA-Consolider Team, CITIMAC, Facultad de Ciencias, Universidad de Cantabria, 39005 Santander, Spain, and [⊥]Departamento de Anatomía y Biología Celular and [∥]Departamento de Biología Molecular, Universidad de Cantabria-IFIMAV, 39011 Santander, Spain

ABSTRACT

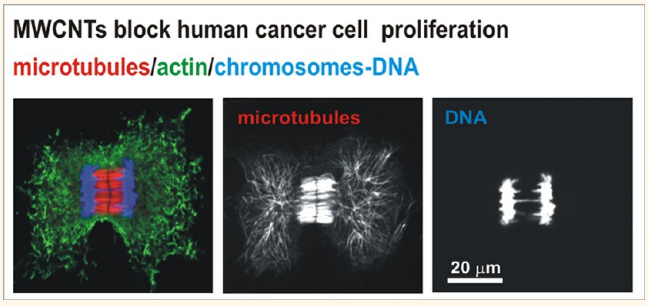

Microtubules are hollow protein cylinders of 25 nm diameter which are implicated in cytokinetics and proliferation in all eukaryotic cells. Here we demonstrate *in vivo* how multiwalled carbon nanotubes (MWCNTs) interact with microtubules in human cancer cells (HeLa) blocking mitosis and leading to cell death by apoptosis. Our data suggest that, inside the cells, MWCNTs display microtubule biomimetic properties, assisting and enhancing noncentrosomal microtubule polymerization and stabilization. These features might be useful for developing a revolutionary generation of chemotherapeutic agents based on nanomaterials.

KEYWORDS: MWCNT · microtubules · cell division · HeLa cell · cancer · apoptosis

Carbon nanotubes (CNTs) represent a class of highly versatile materials that display very interesting mechanical, thermal, and electronic properties.[1,2] Despite this potentiality, their still unknown risks for the environment and living organisms restrict the extensive industrial and commercial applications.[3−5] The use of nanomaterials in medical sciences has the potential to completely transform traditional medicine, producing revolutionary and powerful tools for diagnosis and treatment of diseases. In particular, the application of CNTs in biomedicine is an area of great promise since these nanomaterials are well-known to interact with cells and tissues in living organisms. However, biosynthetic interactions are often a double-edged sword leading to toxicity.

Recent studies suggest that at least 30−50% of functionalized MWCNTs are taken up by cells through an energy-independent process.[6,7] Once inside the cell, CNTs can freely disperse in the cytoplasm, can be included in membranous structures, or can interact with the nuclear envelope, entering the nucleus and binding the DNA.[6−10] These processes have been reported to trigger a plethora of inflammatory, cytotoxic, and genetic alterations producing, among others, DNA clastogenic effects (DNA breakage)[3,11,12] and chromosomal malsegregation (known as aneuploidy).[12−18] However, there is also literature claiming that these nanomaterials could be compatible with the living matter.[10,19−24] Hence, there is an open controversy regarding CNTs' biocompatibility.

This puzzled vision of CNTs' toxicity effects might be a consequence of two major facts: (i) the high diversity of the employed CNTs with different origin and quality, and (ii) the actual dosage of CNTs used in the study. Different types of CNTs display quite distinct physicochemical properties. Lengths and diameters would probably determine their cellular uptake mechanisms and, most likely, their interaction with the different cellular components[25,26] such as intracellular nanofilaments. Among these, there is evidence that CNTs interact with DNA,[27,28] actin,[29] microtubules,[30] and probably intermediate filaments such as the nuclear laminas.[9] These interactions themselves determine the manner with which they interfere with various cellular mechanisms, mostly DNA replication,

* Address correspondence to fanarrag@unican.es, valientr@unican.es.

Received for review January 12, 2012 and accepted July 7, 2012.

Published online July 07, 2012
10.1021/nn302222m

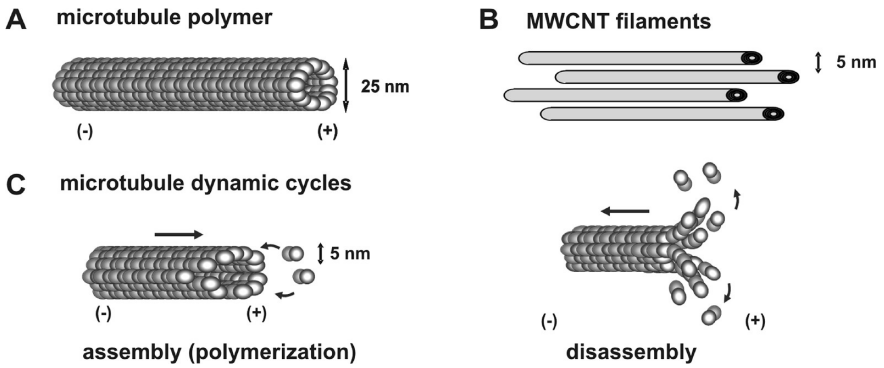

Figure 1. (A) Microtubules are 25 nm diameter protein nanotubes built of 13 protofilaments assembled of tubulin blocks. Due to the polar nature of the tubulin heterodimer, microtubules are polarized polymers that display α-tubulin at their (−) end and β-tubulin at their (+) end. This polarization has important functional implications in dynamics. (B) MWCNTs share several structural characteristics with microtubules (see text). (C) Microtubule polymers continuously undergo assembly/disassembly cycles in a process known as dynamic instability. The (−) end is less dynamic and is located at the centrosome, while the most dynamic end is indicated with the (+) sign. This process is crucial during cell division and tightly regulated by several protein factors *in vivo*.

cell proliferation, and migration. Actin filaments (6 nm diameter) and microtubules (25 nm diameter) play highly conserved roles in cell biology, being required for cell viability, cytokinetics, maintaining the cellular structure, and are crucial at all stages of cell proliferation.[31] These protein polymers are built of actin monomers and tubulin heterodimers, respectively. The soluble-polymerized pools of these proteins coexist in a delicate equilibrium that is controlled by numerous cell factors implicated in the regulation of the cell movement and division mechanisms.

Interestingly, microtubules closely resemble CNTs.[30] Microtubules are naturally occurring nanotubes constituting 13 protein polymers of 5 nm diameter, arranged in a circle (Figure 1). Both CNTs and microtubules self-assemble, have a high length-to-width ratio, display a high resiliency, and both types of filaments form bundles that increase their stiffness. However, in contrast to CNTs, microtubules are continuously switching between phases of assembly (growth) and disassembly (shrinkage) on the time scale of seconds. This dynamic behavior is crucial for cell proliferation, increasing 20- to 100-fold at mitosis.[31] Interference with microtubule dynamics typically results in cell division blockage and chromosomal malsegregation, finally leading to cell death by apoptosis. This explains why microtubules are a target for traditional anticancer drugs such as Taxol or Vinblastine, both antimitotic drugs that bind to microtubules at diverse sites and interfere with microtubule dynamics.[32]

Regarding the dosage effect, many toxicity studies have been done at much higher doses than those acceptable.[33] Moreover, up to now, it is not trivial to determine the concentration of resuspended CNTs in biocompatible solvents. This is mostly due to the high insolubility of these nanomaterials in these solvents[34] and also to the fact that, apparently, dispersed nanotubes often reaggregate and precipitate when diluted into culture media. In this work, we study the effect of the exposure of HeLa cells to well-resuspended multiwalled carbon nanotubes (MWCNTs) in biocompatible media.

RESULTS AND DISCUSSION

MWCNT Characterization and Dispersion. MWCNTs were synthesized following the catalytic chemical vapor deposition method[35] using Co and Mo particles as catalyst. The resulting powder containing MWCNTs was then soaked in an aqueous HCl solution to separate the CNTs. Unlike nitric acid or other oxidizing acids, HCl does not damage the MWCNTs. The acidic suspension was filtered and washed with deionized water several times until neutrality.[35] The as-prepared MWCNTs were characterized by various methods. Figure 2 shows images of transmission electron microscopy (TEM) and atomic force microscopy (AFM) and Raman spectra of the as-prepared MWCNTs. TEM images revealed a population of MWCNTs with a number of walls from 3 to 12, with the outer diameter ranging from 5 to 15 nm and the inner diameter between 2.5 and 10 nm, respectively (Figure 2A). Additionally, most of the MWCNTs displayed an open-end configuration, although occasional capped ends were also observed in approximately 10% of the CNT extremes (9.6% of 125 MWCNT ends). The as-prepared MWCNTs were also characterized by Raman spectroscopy (Figure 2B) where a number of well-characterized MWCNT resonances,[36,37] such as the dispersive disorder induced D band at 1330 cm^{-1}, the tangential G band at 1586 cm^{-1}, and the D′ band at 1614 cm^{-1}, were observed. These were determined using the symmetry analysis[35] to the longitudinal optical mode (LO) close to the Brillouin zone center (Γ) (see Materials and Methods). Both AFM and TEM images revealed bundles of as-prepared MWCNTs of approximately 1.2 to 1.3 μm length (Figure 2C). These techniques

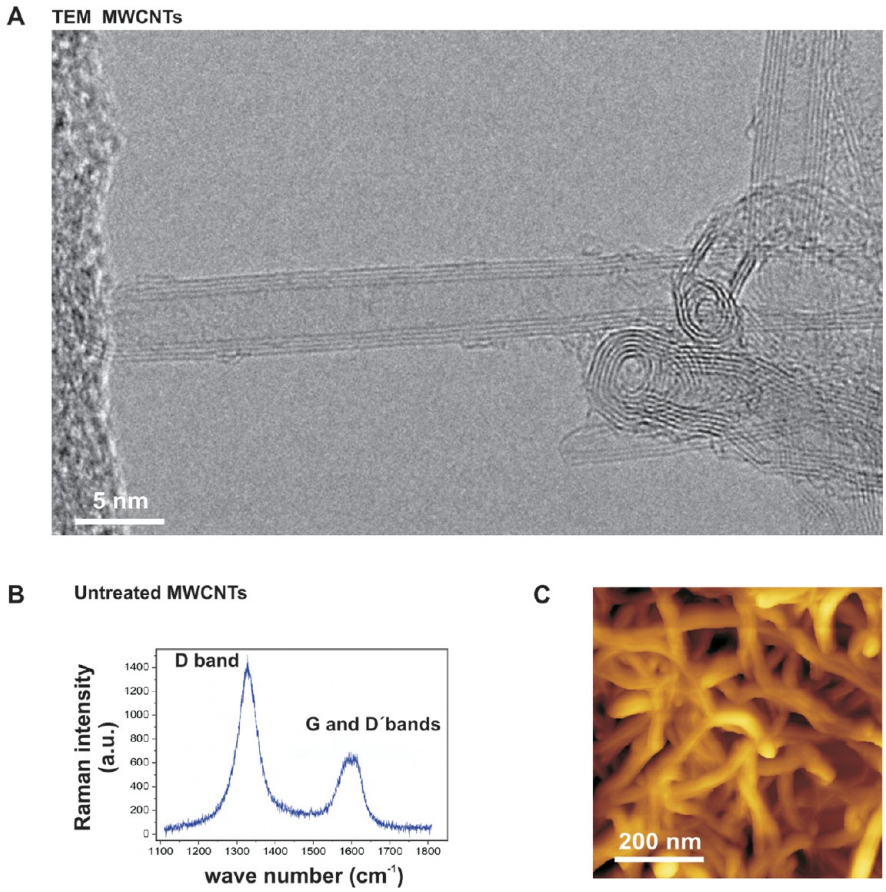

Figure 2. (A) HRTEM image of the as-prepared MWCNTs. (B) Room temperature Raman spectrum of the as-prepared MWCNT using the 647 nm line of an Ar^+–Kr^+ laser. The main peaks are labeled as D, G, and D′ (see text). (C) AFM image of as-prepared MWCNTs forming bundles.

confirmed the absence of undesired impurities on the surface of the MWCNTs.

In order to obtain a stable MWCNT suspension in biocompatible solvents, different media were screened. Among others, we employed sera from different species since this is a standard additive in the culture medium. Serum typically includes high protein and lipid contents, and some of these components have been shown to interact with the surface of various types of CNTs. Some of these are albumin,[38,39] prealbumin,[38] transferrin,[38,39] immunoglobulins,[38] fibrinogen,[39,40] apolipoproteins,[39] and lipids.[41] While we did not get adequate MWCNT resuspension in fetal bovine serum (FBS), and only partial in rabbit serum (RS), we observed that MWCNTs stably dispersed in horse serum (HS) from two different commercial sources (Materials and Methods) (Figure S1). Figure 3 shows the optical absorption spectra of HS with different MWCNT concentrations from 0 to 22.4 μg/mL (A), as well as the Lambert–Beer plot for MWCNTs obtained at 500 nm after subtraction of the HS contribution (B). Similar results have been observed for other wavelengths. We have also included the stability of the 22.4 μg/mL suspension through the temporal evolution of the VIS spectra at 500 nm during a period of 70 h (Figure 3C). The higher MWCNT dispersion ability of HS compared to the other tested sera is likely related to the nonfetal origin of the donor animals. Since serum composition is highly variable and depends on the diet, HS might contain a more suitable composition of apolipoproteins and lipids than other sera, and these components might act as amphipathic molecules functionalizing the MWCNTs.

MWCNTs Enter HeLa and Intermingle with Microtubules. Figure 4 shows live cell images of HeLa cultures treated with a relatively low MWCNT concentration in HS (0.6 μg/mL) for 0, 20, and 70 h as well as identical cells grown for 70 h in a control medium. Important changes in the cell shape, changing from a cobble stone morphology (Figure 4A, HeLa HS control) to a more elongated appearance, are observed. Some cell contours are marked in these images to illustrate the different shapes of cells after 70 h exposure to MWCNTs. The presence of MWCNTs in the culture medium also produced characteristic long cytoplasmic rod-like cell extensions of about 20–60 μm length (white arrows). This cell morphology was observed in 15–20% of the cells 20 h after exposure to MWCNTs and was generalized in 70 h MWCNT-treated cultures. As a general rule, we observed that the higher the dosage, final concentrations ranging from 0.06 to 6 μg/mL,

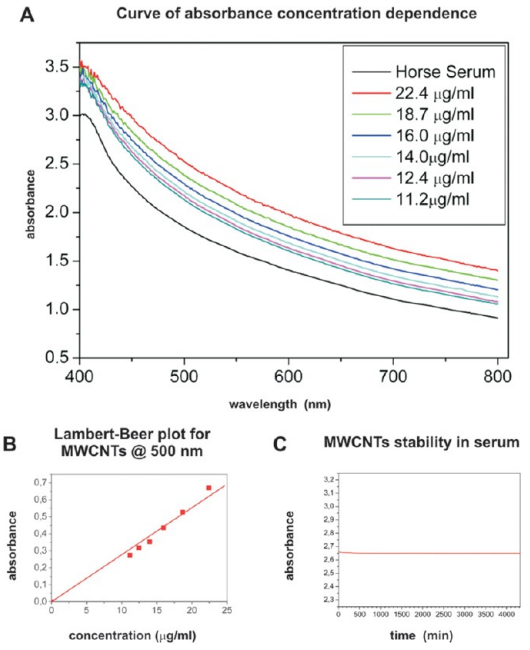

Figure 3. (A) Optical absorption spectra of MWCNTs in HS as a function of concentration. (B) Concentration-dependent absorbance curve for MWCNTS dispersed in HS. The Lambert–Beer plot was obtained subtracting the HS contribution at 500 nm (Figure S1B). (C) Absorbance of MWCNTs at 500 nm as a function of time up to 70 h, demonstrating the stability of the MWCNT suspension.

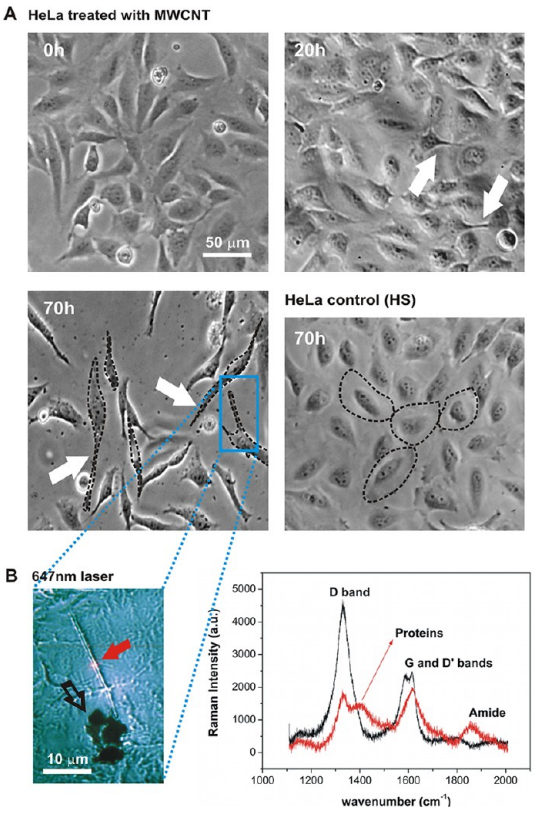

Figure 4. (A) Live cell images of cultures of HeLa cells treated with 0.6 μg/mL of MWCNTs for 0, 20, and 70 h as well as 70 h HeLa control. The profiles of some of the cells in the 70 h cultures have been outlined. The presence of MWCNTs in the culture medium produces long cytoplasmic extensions (white arrows). (B) Image of a HeLa cell extension acquired through the Raman microscope. Laser beam focused on a spot of about 1 μm is marked with a red arrow. Extracellular bundles of MWCNTs were added to the culture media for control (black arrow). Raman scattering experiments performed on the focused HeLa cell cytoplasmic extension (red line) and the extracellular MWCNT (black line). The spectrum detected on the cell extension displays the typical MWCNTs peaks together with signatures that correspond to proteins (Figure S2B).

the more noticeable were all of the observed cellular abnormalities, and the lower the cell survival.

Previous studies from other laboratories have shown that HeLa cells can uptake different CNTs from the media,[9] so we collected the Raman scattering spectra detected on one of these cellular extensions to investigate the presence of MWCNTs (Figure 4B, laser spot is indicated with the red arrow). A Raman spectrum displaying characteristic MWCNT peaks together with new peaks corresponding to typical and distinctive cellular protein and lipids bands was obtained (Figure 4B, red spectrum; Figure S2B). We observe the extended amide III mode corresponding to the coupled C–H, N–H deformation modes and peptide shoulder at 1392 cm^{-1}, the CH_2 and CH_3 deformations mode at 1484 cm^{-1}, and the amide I mode at 1650 cm^{-1} (Figure S2B). For comparison, we include the Raman spectra of a MWCNT aggregate (black empty arrow, black spectrum) used as a control within the culture medium. These results confirmed the presence on MWCNTs in these abnormal cytoplasmic extensions.

Microtubule stabilization by biological means produces similar cell shape changes in HeLa cells.[42] So we investigated by immunofluorescence with antibodies against tubulin the presence of microtubules in these cytoplasmic extensions. Figure S2A shows the existence of bundles of microtubules (red channel) within one of these extensions. This finding suggests microtubules are stabilized by MWCNTs, producing bundles that protrude and grow these cell extensions, but this is only possible if MWCNTs are intracellular.

Figure 5 shows a TEM image of a section of a HeLa cell treated with MWCNTs in the culture medium for 70 h. Several bundles of intracellular MWCNTs (red arrows) intermingling with microtubules (white arrows) are observed surrounding the nucleus. A diagram of the sample preparation is also shown. MWCNT bundles were also sometimes found surrounded by a membrane (Figure S3A) and within the nucleus interacting with the chromatin as previously reported and described by other authors (data not shown).[3,6,8–11] These findings confirm that MWCNTs are inside cells.

MWCNTs Interfere with the Microtubule Dynamics and Block Cell Proliferation, Leading to Apoptosis. Nanomaterials and, in particular, CNTs have been blamed for disrupting mitosis, producing aberrant mitotic spindles.[4,15] Moreover, SWCNTs have been observed in close association with the spindle microtubules and centrosomes.[43]

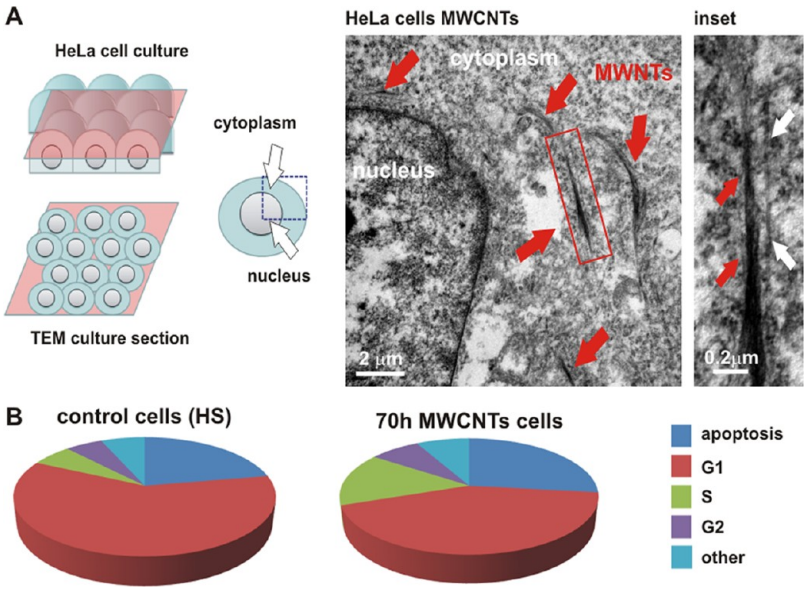

Figure 5. (A) Diagram of the cell processing for TEM. Cutting plane is shown in pink. Transmission electron micrograph (TEM) of a section of a HeLa cell. Several bundles of MWCNTs (red arrows) are observed inside the cell. (Inset) Higher magnification of a MWCNT bundle (red arrows) with a microtubule running parallel (white arrows). (B) Pie charts displaying the proportions of cells at different stages of the mitotic cycle and apoptosis (dark blue) in 70 h control or MWCNT-treated cultures. This analysis has been performed by flow cytometry (Figure S4A). A drop of cells at the G1 stage (nondividing cells, red), a rise of cells at S-G2 (dividing cells, green/purple), and a higher rate of apoptosis (5% rise by flow cytometry) are all hallmarks of a cell proliferation blockage.

Figure 5B represents the quantification of HeLa cells at different stages of the proliferating cell cycle using flow cytometry (Figure S4).[44] Pie charts are shown for simplicity. A drop of cells at the G1 stage (nondividing cells, red) and a rise of cells at S-G2 stages (dividing cells, green-purple) are observed in HeLa cells exposed to MWCNTs for 70 h. Flow cytometry experiments also revealed a 5% rise in the apoptotic events (dying cells, dark blue) in MWCNT-treated cells compared to control cells (Figure S4). This value is routinely considered significant in the conditions of the study. Similar results were obtained by direct morphological quantification on growing cell cultures. All of these remarkable changes are indicative of a cell proliferation blockage and suggest that MWCNTs interfere with cell proliferation in HeLa cells, retarding or blocking the cell division process.

The interaction of MWCNTs with the microtubule cytoskeleton in these cells was studied by tubulin immunostaining and confocal microscopy examination. Immunofluorescence on these cultures revealed that MWCNT treatment produced a broad spectrum of aberrations occurring at all mitotic stages. Apart from the previous reported DNA clastogenic effects,[3,11,12,27,28] we could confirm important microtubular defects, mostly microtubule spindle and anaphase/telophase aberrations. Figure 6A displays images of different samples of the aberrant spindle microtubules (red) and chromosomal distributions (blue) found in MWCNT-treated cells, including double spindles, unfocused spindle microtubules, multipolar spindles, and, finally, monoastral spindles (left to right). These abnormal spindle configurations are typically attributed to microtubule defects. Figure 6B,C show abnormal telophase and anaphase images, respectively. Tripolar telophases (left) or asymmetric cell divisions (right, one cell with two nuclei, blue arrows) are also observed. Figure 6C (right panel) shows the disposition of the microtubule cytoskeleton in an anaphase cell (observed in red in the color image). Here the abnormally high density and excess bundling of midzone microtubules (white arrow) is accompanied with a complete disorganization of the astral microtubules (red arrows) that should connect the centrosomes to the cell cortex (astral microtubules). All of these abnormal mitotic images typically lead to asymmetric mitosis or mitotic arrest and eventually cell death by apoptosis.

MWCNTs Display Biomimetic Properties Behaving as Tubulin Nucleation Templates and Interfering with Microtubule Dynamics *in Vivo*. As mentioned above, in terms of molecular architecture and cell mechanisms, microtubules and nanotubes are very similar, and it is likely that they interact. During cell division, microtubule dynamics increases 20- to 100-fold[31] when the microtubule cytoskeleton reorganizes completely to assemble the mitotic spindle. The above results suggest that MWCNTs interfere with microtubule dynamics. We now questioned if MWCNTs could behave biomimetically *in vivo* and directly interact with microtubules. For this purpose, we investigated tubulin polymerization speed and trajectories in live cells (see Materials and Methods).

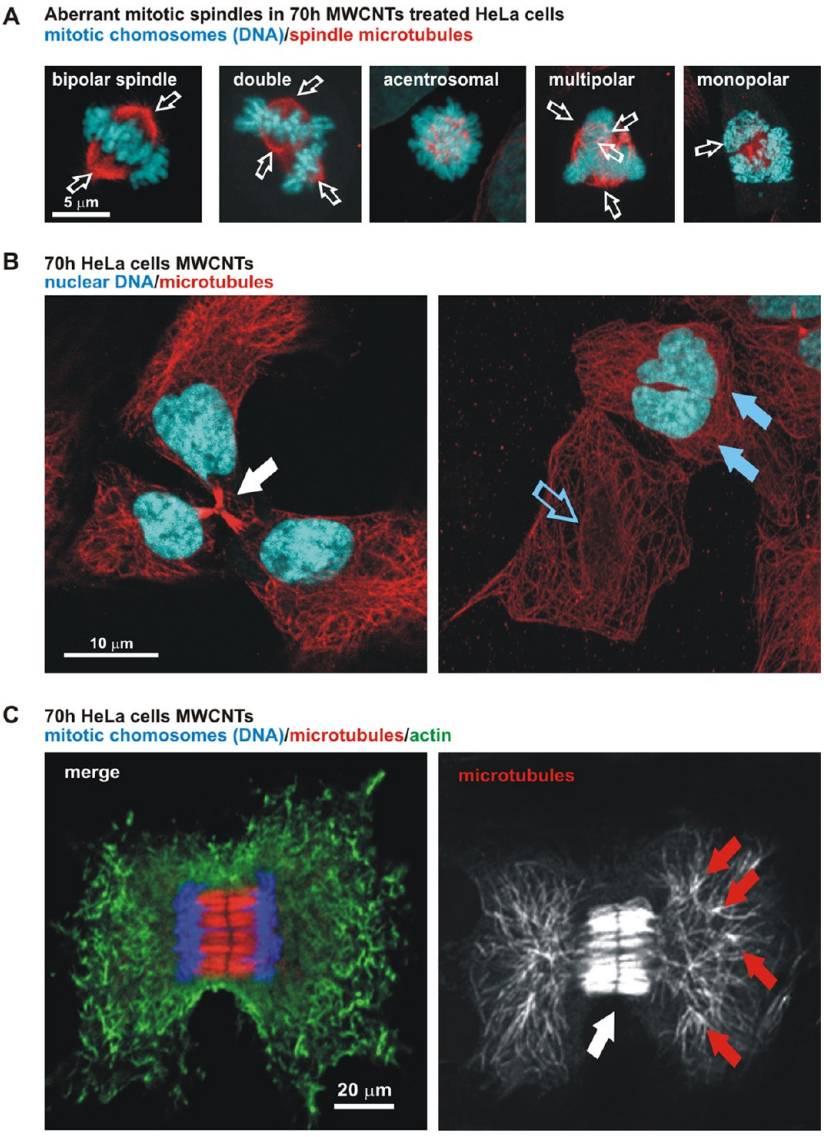

Figure 6. (A) Confocal microscopy projection images of aberrant mitotic spindles in cells treated with MWCNTs. Aberrations in the organization of the spindle microtubules (red channel) and chromosomal distribution (blue channel) are observed. Centrosomes, where present, are indicated by white arrows (see the text). (B) Anaphase/telophase aberrations in MWCNT-treated cultures. Defects include tripolar (left, white arrow) and asymmetric cell divisions (right), where the two nuclei of daughter cells move to one of the cells (filled blue arrows/empty blue arrow). (C) Confocal microscopy projection image of an anaphase. No obvious changes in the actin filaments (green channel) are detected, and abnormally high density of midzone microtubules (red channel extracted in gray, white arrow) and acentrosomal microtubule irradiation (red arrows) are observed (see the text).

In Figure 7, confocal microscopy projection images were obtained in living cells where *de novo* microtubule trajectories are highlighted. For the sake of clarity, we have emphasized some centrosomal microtubules as red lines and noncentrosomal microtubules as blue lines. The centrosome localization is marked by a red arrow. Figure 7A shows microtubule trajectories in control cells, where most *de novo* microtubules irradiate from the centrosome (red trajectories). On the other hand, in cells grown in the presence of MWCNTs for 70 h (Figure 7B), most of *de novo* microtubule trajectories are not connected to the centrosome (blue trajectories) (Supporting Information, movies). This study demonstrates that MWCNTs interfere with microtubule nucleation sites and trajectories, disrupting microtubule irradiation from the centrosome. This is a chief finding since *in vivo* microtubules typically irradiate from the centrosome toward the periphery of the cell.[45]

On the other hand, statistical analysis of the tubulin polymerization speed on live cells (see Materials and Methods) revealed that microtubule nucleation was not significantly affected in terms of total growth (Figure S4B) in MWCNT-treated cells, with a calculated average growing speed of approximately 4 μm/min for both conditions.

In Figure 8, we reproduce a classical microtubule depolymerization−repolymerization study on live cells

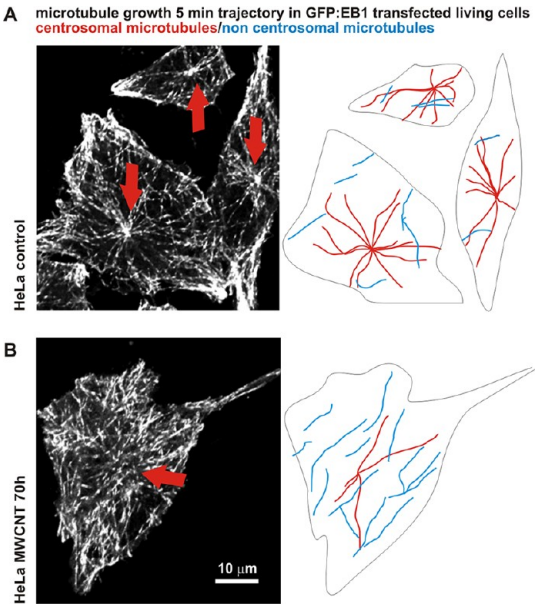

Figure 7. Five minute time-lapse confocal projection image showing the trajectories of GFP:EB1 *de novo* labeled microtubules in live cells (see Materials and Methods). (A) In control HeLa, most microtubules irradiate from the centrosome (red lines). (B) In MWCNT-treated cells, only occasional microtubules irradiate from the centrosome, and most microtubules are acentrosomal (blue lines). Cellular contours are outlined in black.

(see Materials and Methods).[46] Figure 8A gives an overview of the experiment where cellular microtubules (red) are first depolymerized completely as explained in Materials and Methods and how, when cells are next exposed to permissive conditions, microtubules typically regrow from the centrosome (red star). Cell nuclei are colored in blue.

Figure 8B shows a confocal fluorescent image of four cells after the microtubule disassembly process. Naked centrosomes (indicated by white arrows) are observed after the complete microtubule disassembly process. A single tubulin spot is visible in both treated and untreated cells. Figure 8C plots the kinetics of microtubule regrowth after exposure to permissive conditions during the indicated times in control cells (black line) and MWCNT-treated cells (blue line). Highly significant differences in total microtubule densities are already observed at t = 5 min. Figure 8D shows microtubule repolymerization in MWCNT-treated cells (1) and control (2) at this time point. While in MWCNT-treated cells microtubule repolymerization is remarkable, in control cells, repolymerization is only observable as small asters irradiating from the centrosome. This unusually fast microtubule reassembly corroborated that intracellular MWCNTs interfered with microtubule polymerization, significantly enhancing the tubulin polymerization speed. Tubulin–CNT hybrid structures have also been produced *in vitro*, where a patent nanotube-directed tubulin polymerization has been reported.[47]

Finally, Figure 9 includes high-resolution confocal images of the above cells 2 min after recovery. At this time point, control cells display naked centrosomes (inset, red arrows), while 70 h MWCNT-treated cells display abundant small microtubule polymers throughout the cytoplasm. Centrosome-independent microtubule polymerization is triggered throughout the cell cytoplasm (inset, white arrows). This random microtubule nucleation suggests that MWCNTs behave as biomimetic filaments that enhance tubulin polymerization *in vivo*, serving as tubulin nucleating scaffolds.

According to all of the above findings, we propose the microtubule–MWCNT interaction models depicted in Figure 10. In the "microtubule–MWCNT mixed bundle" model (Figure 10A, left), bundles of MWCNTs longitudinally associate with microtubules. In the "biomimetic microtubule" model (Figure 10A, right), one (or various) of the 13 protofilaments is substituted by MWCNTs in the microtubule. The biomimetic microtubule model is based on the similar diameters of tubulin protofilaments and MWCNTs (approximately 5 nm). The combination of carbon nanotubes and tubulin protofilaments would restrict microtubule dynamics and increase the stability of these biosynthetic nanotubules. Both models will, first, enhance microtubule bundling in nondividing cells, leading to the formation of abnormal cellular extensions, and, second, will fatally interfere with microtubule dynamics in mitosis, leading to cell division arrest and death by apoptosis.

SUMMARY

Our data demonstrate that MWCNTs invade the HeLa cell cytoplasm, associate with microtubules, and behave as tubulin scaffolds, promoting tubulin nucleation and microtubule assembly while reducing microtubule dynamics. MWCNT–microtubule interactions alter the delicate growth/shrinkage equilibrium that microtubules normally display, leading to aberrant cell morphologies and dramatic consequences during cell division. These findings elucidate how MWCNTs interfere with various cell biology processes, but more particularly how these fibers produce mitotic spindle aberrations and all of the consequences that are derived from this fact, such as chromosomal malsegregation and aneuploidy. Since microtubules and actin filaments are targets of a growing number of anticancer drugs, the understanding of the relationship between MWCNTs and microtubules *in vivo* could drive bionanotechnology a step closer toward a next generation of biocompatible materials for chemotherapy. MWCNTs, by themselves, could be ideal nanomedicines for cancer treatment since they are capable of penetrating mammalian cell membranes and interfering with both the proliferative and migratory cellular mechanisms.

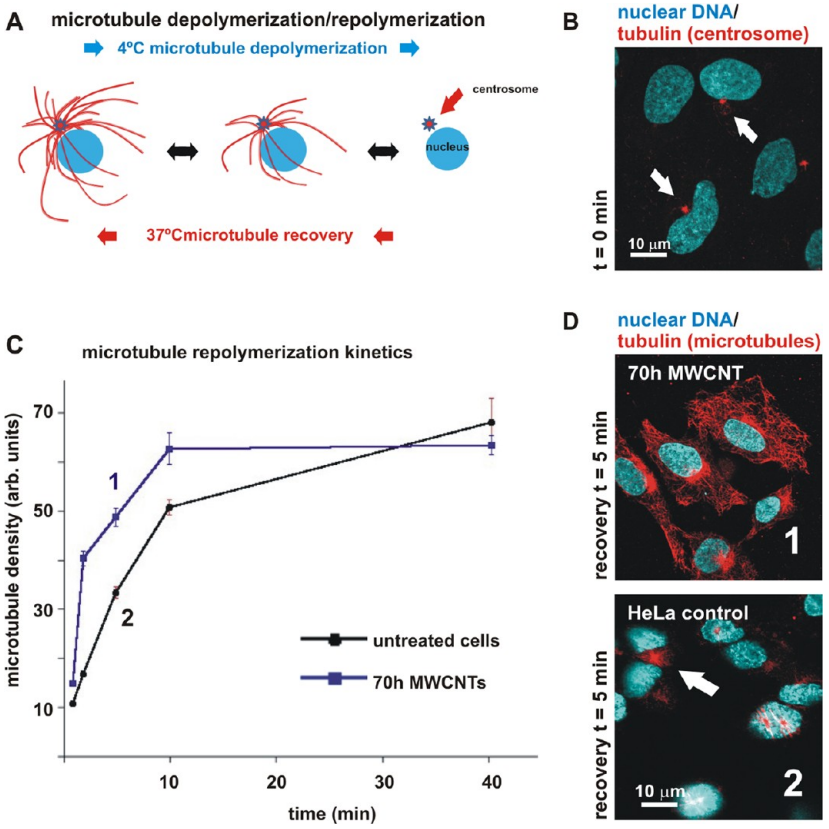

Figure 8. (A) Diagram of the depolymerization−repolymerization experiment performed in live cells (described in Materials and Methods). Cellular microtubules (red) are first depolymerized completely. Under permissive conditions, microtubules typically regrow from the centrosome (red star) until complete cytoskeletal recovery. Cell nuclei are shown in blue. (B) Tubulin labeling with fluorescent antibodies (immunostaining) in cold treated cells shows a complete microtubule disassembly in both MWCNT-treated and control cells (not shown). Naked centrosomes, labeled with antitubulin antibodies, are indicated by white arrows. (C) Kinetics of microtubule regrowth at the indicated times in control cells (black line) and MWCNT-treated cells (blue line). (D) Remarkable differences in the temporal evolution of microtubule densities are observed for control HeLa and MWCNT-treated cells. Confocal microscopy images (1, 2) of cultures 5 min after permissive conditions. (1) MWCNT-treated cells display a faster microtubule nucleation than controls (2), where only a small centrosomal microtubule aster is observed (white arrow).

Further studies will seed new light on determining the maximum biocompatible dosage of these nanomaterials and different vectorization methods, which may allow MWCNTs to be suitable as a cancer treatment.

MATERIALS AND METHODS

MWCNT Functionalization and Dispersion. MWCNTs were dispersed by repeated cycles of vortex mixing followed by mild sonication (cycles of 10 min, frequency of 38 kHz). Increasing volumes of serum from different species were employed. FBS was obtained from Gibco-Life Technologies (Cat No. 10108165). Rabbit serum was produced in our laboratories, and HS was obtained commercially from Gibco-Life Technologies (Cat No. 16050122) and PAA-GE Life Sciences (Cat No. B15-021). A stock solution containing 0.140 mg of MWCNTs dispersed in 2.3 mL of HS was prepared (60 μg/mL), after that, the sample was subjected to three cycles of 10 min sonication in an Elmasonic SH-15 water bath (frequency 38 kHz) at room temperature. The stability of the suspension and the existence of aggregates were tested through the optical absorption spectra in the 400−800 mn range for 20 min after each sonication cycle. A total of three cycles were sufficient to obtain a well-dispersed solution containing up to 60 μg/mL MWCNTs (stock solution). Higher concentrations of MWCNTs were impossible to disperse or finally precipitated. Intermediate centrifuge or decantation steps to remove large aggregates were avoided in order to maintain the original MWCNT concentration.

Transmission Electron Microscopy. Morphological characterization of the as-prepared MWCNTs was done in a JEOL JEM 2100 transmission electron microscope operating at 120 kV. Samples for TEM were prepared as described for SWCNTs[44] using ethanol as dispersant and omitting the sample centrifugation steps. A drop of this suspension was adsorbed onto a Lacey copper grid. Electron microscopy on cells (JEOL JEM 1011 microscope) was performed on 70 nm Araldite sections of pellets of HeLa cells fixed with 1% glutaraldehyde in 0.12 M phosphate buffer, washed in 0.12 M phosphate buffer, postfixed in 1% buffered osmium tetroxide, dehydrated in a graded acetone series, embedded in Araldite, and stained with lead citrate and uranyl acetate.

HeLa Cell Cultures. HeLa cells, an immortalized human cervical cancer cell line, were grown in DMEM media containing 10% FCS at 37 °C, 5% CO_2. Unless otherwise indicated, cells were exposed to 0.6 μg/mL MWCNTs in the culture medium for 70 h. Control cells were treated with identical HS amounts (a 1:1000 v/v). The culture medium conditions do not significantly differ from standard cell growth conditions.

Optical and Raman Spectroscopy. Visible absorption spectra were recorded with Cary 50 and Cary 6000i spectrometers

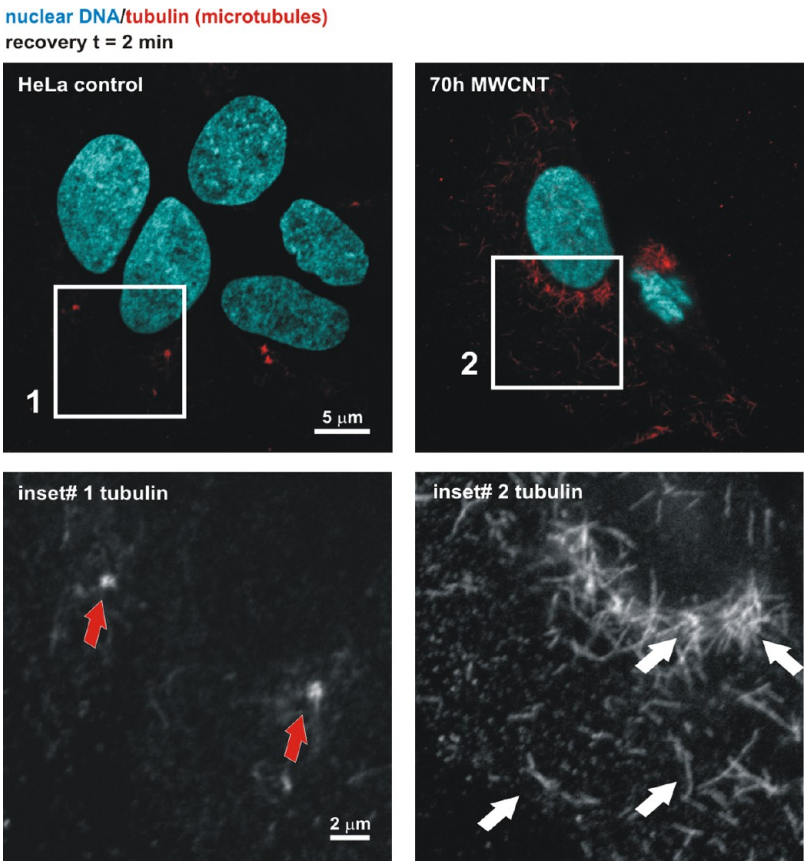

Figure 9. High-resolution confocal images of control and MWCNT-treated cells allowed to regrow microtubules for 2 min (red and gray channels). (Inset #1) While control cells display naked centrosomes (red arrows), (inset #2) 70 h MWCNT-treated cells display abundant microtubule nucleation throughout the cytoplasm. Several centrosome independent microtubule polymerization sites are observed (white arrows).

(Varian) operating between 400 and 800 nm. A quartz cuvette of 1 cm light path was filled with solutions of different concentrations of MWCNTs suspended in HS. The unpolarized Raman spectra were taken with a Horiba T64000 triple spectrometer in the backscattering geometry, using the 647 nm line of a Coherent Innova Spectrum 70C Ar^+–Kr^+ laser and a nitrogen-cooled CCD (Jobin-Yvon *Symphony*) with a confocal microscope for detection. The laser beam was focused down to 1 μm spot with a 100× objective and kept the power on the sample below 2 mW to avoid laser-heating effects on the probed material and the concomitant softening of the observed Raman peaks. MWCNT concentric graphene sheets produce a characteristic Raman spectrum distinguishable from the SWCNT spectrum.[37] The radial breathing modes (RBM), a Raman feature associated with a small diameter inner tube, are not common and can only sometimes be observed when a good resonance condition is established. The RBM signal from large diameter tubes is usually too weak to be observable and the ensemble average of inner tube diameter broadens the signal.

Immunostaining and Confocal Microscopy Imaging. Cells were fixed in 1% glutaraldehyde. Autofluorescence was quenched with 1% sodium borohydride. Antibodies used were anti-α-tubulin (B512) (Sigma-Aldrich) combined with a secondary goat anti-mouse IgG antibody conjugated with CY3 (Jackson ImmunoResearch Laboratories Inc.) or Alexa Fluor 488 (Molecular Probes, Invitrogen). Actin was stained with phalloidin–tetramethylrhodamine B isothiocyanate (Sigma-Aldrich) and DNA (nucleus and chromosomes) with Hoechst dye (Bisbenzimide) (Sigma-Aldrich). Confocal microscopy images were obtained with a Nikon A1R confocal microscope and processed with the NIS-Elements Advanced Research software. All confocal cell images are pseudocolored.

Flow Cytometry. Flow cytometry was performed on a suspension of fixed HeLa cells stained with Hoechst using a Becton Dickinson FACS Cantoll equipment. This dye produces a quantitative staining of DNA. This technique was used to determine a blockage in cell proliferation (the DNA content of per cell is doubled during the cell cycle) and also to quantify the fractional DNA content ("sub-G1" peak), indicative of apoptosis. Further details of the technique can be found in ref 44. Analysis was performed on an average of 10 000 cells per condition (HS control or MWCNT-treated cells). Data were analyzed using the FACS Diva software (Becton Dickinson, NJ, USA), and the proportions of the different cell populations including apoptotic cells are represented in a pie chart (Figure 5). Original flow cytometry graphs are shown in Figure S4A.

***In Vivo* Microtubule Experiments.** Microtubule dynamic instability is controlled, among others, by a protein that binds this extreme of the microtubule known as EB1. Fluorescent mutants of this protein can be used to investigate microtubule dynamics[48] and are also a way to determine the trajectory and speed of microtubule growth in cultures of living HeLa cells. Microtubule nucleation speed and trajectories were assessed in HeLa cells transfected with a vector expressing GFP:EB1 kindly provided by Dr. Akhmanova (Utrecht University, The Netherlands). This fluorescent protein only labels growing microtubule tips in live cells as described elsewhere.[48] Transfection was performed with SuperFect Transfection Reagent (Quiagen, Life Sciences) following the manufacturer's protocols 24 h before exposure to MWCNTs in the medium. Microtubule nucleation speed was assessed in 70 h treated and control live cells by confocal microscopy on a fixed single *Z* plane that coincided with the centrosome. Figure 7 shows single (*X*, *Y*, *t*) projection images of 5 min time lapse movies (at 10 s/frame, total 30 frames) where the length of the microtubules corresponds to the total microtubule growth

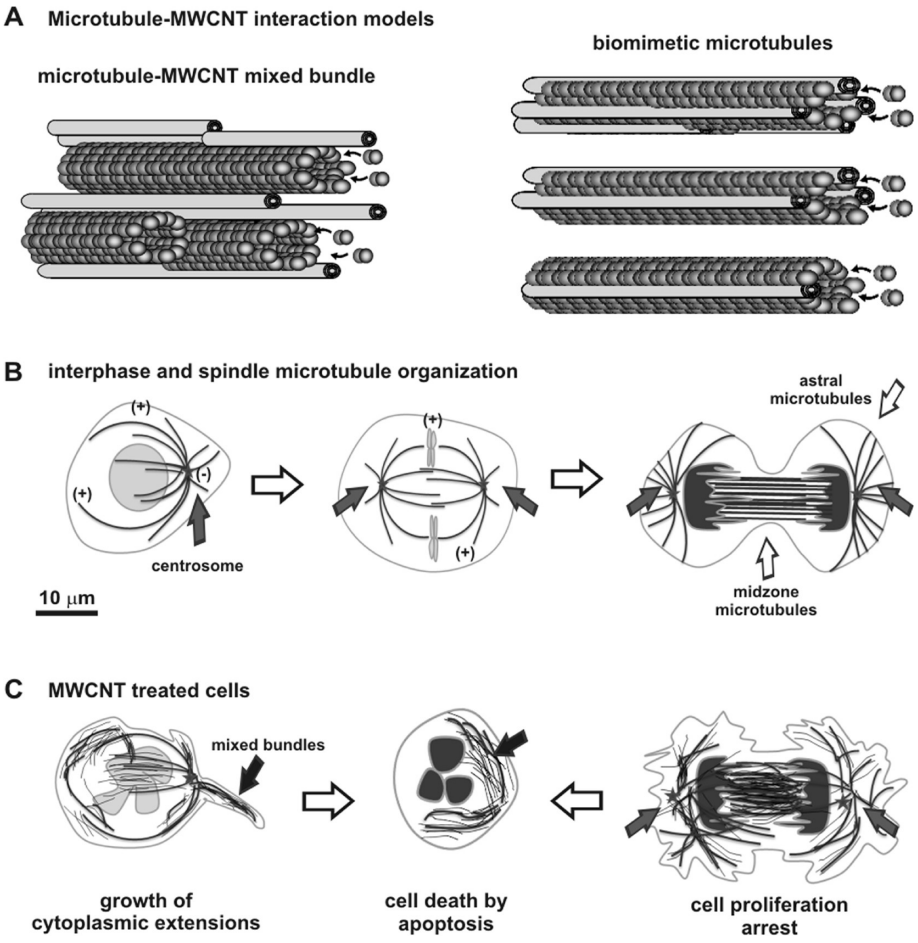

Figure 10. (A) Microtubule−MWCNT interaction models. In the microtubule−MWCNT mixed bundle, bundles of MWCNTs longitudinally associate with microtubules, restricting microtubule dynamics. The biomimetic microtubule model is based on the similar diameters of tubulin protofilaments and MWCNTs. Here, one (or various) of the 13 protofilaments is substituted by MWCNTs in the microtubule. This combination of nanotubes/protofilaments increases the stability of this biosynthetic nanotubule. (B) Diagram of a normal microtubule network (blue) irradiating from the centrosome (gray arrow) in interphase (G0) cells. Microtubule polarity is indicated with the (−) and (+) signs. (Center) During early mitosis, centrosomes duplicate (gray arrows) and microtubules, still irradiating from the centrosome, reorganize into a spindle connecting to chromosomes. (Right) During anaphase, astral and midzone microtubules (empty arrows) generate sliding forces to separate daughter cells. (C) In the presence of intracellular MWCNTs (thin filaments), the microtubule network does not irradiate from the centrosome and forms MWCNT−microtubule mixed bundles (black arrows) that can protrude, generating cytoplasmic extensions or fatally interfere with microtubule dynamics in mitosis, leading to cell division arrest and death by apoptosis (center).

for the time frame (5 min). Trajectory identification was performed on the projection images, drawing lines connecting successive points for each microtubule track. *De novo* microtubule growth was quantified as explained above.

Microtubule Depolymerization−Repolymerization Experiments. The microtubule tubulin polymer disassembles under low-temperature conditions (4 °C, 30 min), repolymerizing as soon as they are back to permissive temperatures (37 °C).[46] Microtubule depolymerization was performed with culture medium at 4 °C, containing 2 μM nocodazole for 30 min. Microtubule regrowth was performed placing coverslips into fresh media at 37 °C for the indicated times. Cells were snap fixed in 1% glutaraldehyde at the indicated times and immunostained against tubulin as explained above.

Measurements and Statistical Analysis. EB1 life cell microtubule total growth was quantified on GFP:EB1 transfected cells (50 treated cells and 75 untreated cells) on random confocal images obtained with a Plan Fluor 40× oil NA 1.3 objective. Microtubule repolymerization kinetics was quantified 2, 5, 10, and 40 min after permissive conditions in an average of 20 cells for each condition and at each time point. The significance level taken was $p < 10^{-2}$. The highly significant level taken was $p < 10^{-5}$. Images were quantified with the ImageJ 1.36b, Wayne Rasband NIH (USA) software. Digitalized images were converted to binary and automatically segmented using a histogram derived thresholding method based on a median algorithm as starting point. A *t*-test statistical analysis was carried out to evaluate the significance of these results. Graphs and *t*-test analysis were carried out with standard commercial software. Quantitative results are expressed as mean values and standard error bars.

Conflict of Interest: The authors declare no competing financial interest.

Acknowledgment. We thank L. Alvarez for her technical help, and Prof. J. C. Zabala for his support and helpful scientific discussions. We are grateful to the Nikon A1R Laser Microscopy Unit of the IFIMAV Institute for the confocal microscopy. This work has been supported by the Spanish MICINN under Projects ref. MAT2011-28868-C02-01; BFU2010-18948, MALTA Consolider-Ingenio ref. CSD2007-00045 and Centrosome-3D Consolider-Ingenio ref. CSD2006-00023. We thank AIST-NT International for their help with the AFM study.

Supporting Information Available: Additional figures and movies. This material is available free of charge *via* the Internet at http://pubs.acs.org.

REFERENCES AND NOTES

1. Bianco, A.; Kostarelos, K.; Prato, M. Applications of Carbon Nanotubes in Drug Delivery. *Curr. Opin. Chem. Biol.* **2005**, *9*, 674–679.
2. Schnorr, J. M.; Swager, T. M. Emerging Application of Carbon Nanotubes. *Chem. Mater.* **2011**, *23*, 646–657.
3. Lin, Y.; Taylor, S.; Li, H.; Fernando, S. K. A.; Qu, L.; Wang, W.; Gu, L.; Zhou, B.; Sun, Y. P. Advances towards Bioapplications of Carbon Nanotubes: Using Carbon Nanotubes To Induce Micronuclei and Double Strand Breaks of the DNA in Human Cells. *J. Mater. Chem.* **2004**, *14*, 527–541.
4. Oberdöster, G. Safety Assessment for Nanotechnology and Nanomedicine: Concepts of Nanotoxicology. *J. Intern. Med.* **2010**, *267*, 89–105.
5. Krug, H. F.; Wick, P. Nanotoxicology: An Interdisciplinary Challenge. *Angew. Chem., Int. Ed.* **2011**, *50*, 1260–1278.
6. Lacerda, L.; Russier, J.; Pastorin, G.; Herrero, M. A.; Venturelli, E.; Dumortier, H.; Al-Jamal, K. T.; Prato, M.; Kostarelos, K.; Bianco, A. Translocation Mechanisms of Chemically Functionalised Carbon Nanotubes Across Plasma Membranes. *Biomaterials* **2012**, *33*, 3334–3343.
7. Shi, X.; Von dem Bussche, A.; Hurt, R. H.; Kane, A. B.; Gao, H. Cell Entry of One-Dimensional Nanomaterials Occurs by Tip Recognition and Rotation. *Nat. Nanotechnol.* **2011**, *6*, 714–719.
8. Porter, A. E.; Gass, M.; Muller, K.; Skepper, J. N.; Midgley, P. A.; Welland, M. Direct Imaging of Single-Walled CNTs in Cells. *Nat. Nanotechnol.* **2007**, *2*, 713–177.
9. Yehia, H. N.; Draper, R. K.; Mikoryak, C.; Walker, E. K.; Bajaj, P.; Musselman, I. H.; Daigrepont, M. C.; Dieckmann, G. R.; Pantano, P. Single-Walled Carbon Nanotube Interactions with HeLa Cells. *J. Nanobiotechnol.* **2007**, *23*, 5–8.
10. Mooney, E.; Dockery, P.; Greiser, U.; Murphy, M.; Barron, V. CNTs and Mesenchymal Stem Cells: Biocompatibility, Proliferation and Differentiation. *Nano Lett.* **2008**, *8*, 2137–2143.
11. Muller, J.; Decordier, I.; Hoet, P. H.; Lombaert, N.; Thomassen, L.; Huaux, F.; Lison, D.; Kirsch-Volders, M. Clastogenic and Aneugenic Effects of Multi-Wall CNTs in Epithelial Cells. *Carcinogenesis* **2008**, *29*, 427–433.
12. Cveticanin, J.; Joksic, G.; Leskovac, A.; Petrovic, S.; Sobot, A. V.; Neskovic, O. Using CNTs To Induce Micronuclei and Double Strand Breaks of the DNA in Human Cells. *Nanotechnology* **2010**, *21*, 015102.
13. Di Giorgio, M. L.; Di Bucchianico, S.; Ragnelli, A. M.; Aimola, P.; Santucci, S.; Poma, A. Effects of Single and Multi Walled CNTs on Macrophages: Cyto and Genotoxicity and Electron Microscopy. *Mutat. Res.* **2011**, *722*, 20–31.
14. Sargent, L. M.; Shvedova, A. A.; Hubbs, A. F.; Salisbury, J. L.; Benkovic, S. A.; Kashon, M. L.; Lowry, D. T.; Murray, A. R.; Kisin, E. R.; Friend, S.; *et al.* Induction of Aneuploidy by Single-Walled Carbon Nanotubes. *Environ. Mol. Mutagen.* **2009**, *50*, 708–717.
15. Gonzalez, L.; Decordier, I.; Kirsch-Volders, M. Induction of Chromosome Malsegregation by Nanomaterials. *Biochem. Soc. Trans.* **2010**, *38*, 1691–1697.
16. Kisin, E. R.; Murray, A. R.; Sargent, L.; Lowry, D.; Chirila, M.; Siegrist, K. J.; Schwegler-Berry, D.; Leonard, S.; Castranova, V.; Fadeel, B.; *et al.* Genotoxicity of Carbon Nanofibers: Are They Potentially More or Less Dangerous Than CNTs or Asbestos? *Toxicol. Appl. Pharmacol.* **2011**, *252*, 1–10.
17. Bottini, M.; Bruckner, S.; Nika, K.; Bottini, N.; Belluci, S.; Magrini, A.; Bargamaschi, A.; Mustelin, T. Multi-Walled Carbon Nanotubes Induced T Lymphocyte Apoptosis. *Toxicol. Lett.* **2006**, *160*, 121–126.
18. Pulskamp, K.; Diabaté, S. CNTs Show No Sign of Acute Toxicity but Induce Intracellular Reactive Oxygen Species in Dependence on Contaminant. *Toxicol. Lett.* **2007**, *168*, 58–74.
19. Chin, S. F.; Baughman, R. H.; Dalton, A. B.; Dieckmann, G. R.; Draper, R. K.; Mikoryak, C.; Musselman, I. H.; Poenitzsch, V. Z.; Xie, H.; Pantano, P. Amphiphilic Helical Peptide Enhances the Uptake of Single-Walled CNTs by Living Cells. *Exp. Biol. Med.* **2007**, *232*, 1236–1244.
20. Zhang, X.; Meng, L.; Lu, Q. Cell Behaviors on Polysaccharide-Wrapped Single-Wall Carbon Nanotubes: A Quantitative Study of the Surface Properties of Biomimetic Nanofibrous Scaffolds. *ACS Nano* **2007**, *3*, 3200–3206.
21. Malarkey, E. B.; Parpura, V. CNTs in Neuroscience. *Acta Neurochir. Suppl.* **2010**, *106*, 337–341.
22. Ryoo, S. R.; Kim, Y. K.; Kim, M. H.; Min, D. H. Behaviors of NIH-3T3 Fibroblasts on Graphene/Carbon Nanotubes: Proliferation, Focal Adhesion, and Gene Transfection Studies. *ACS Nano* **2010**, *4*, 6587–6598.
23. Leeuw, T. K.; Reith, R. M.; Simonette, R. A.; Harden, M. E.; Cherukuri, P.; Tsyboulski, D. A.; Beckingham, K. M.; Weisman, R. B. Single-Walled CNTs in the Intact Organism: Near-IR Imaging and Biocompatibility Studies in Drosophila. *Nano Lett.* **2007**, *7*, 2650–2654.
24. Lobo, A. O.; Antunes, E. F.; Machado, A. H. A.; Pacheco-Soares, C.; Trava-Airoldi, V. J.; Corat, E. J. Cell Viability and Adhesion on As-Grown Multi-Wall Carbon Nanotube Films. *Mater. Sci. Eng., C* **2007**, *28*, 264–269.
25. Raffa, V.; Cioffani, G.; Nitodas, S.; Karachalios, T.; D'Alessandro, D.; Masini, M.; Cuschieri, A. Can the Properties of Carbon Nanotubes Influence Their Internalization by Living Cells? *Carbon* **2008**, *46*, 1600–1610.
26. Raffa, V.; Cioffani, G.; Vittorio, O.; Riggio, C.; Cuschieri, A. Physicochemical Properties Affecting Cellular Uptake of Carbon Nanotubes. *Carbon* **2010**, *46*, 1600–1610.
27. Li, X.; Peng, Y.; Qu, X. CNTs Selective Destabilization of Duplex and Triplex DNA, Inducing B-A Transition in Solution. *Nucleic Acids Res.* **2006**, *34*, 3670–3676.
28. Li, X.; Peng, Y.; Ren, J.; Qu, X. Carboxyl-Modified Single-Walled CNTs Selectively Induce Human Telomeric i-Motif Formation. *Proc. Natl. Acad. Sci. U.S.A.* **2006**, *103*, 19658–19663.
29. Holt, B. D.; Short, P. A.; Rape, A. D.; Wang, Y. L.; Islam, M. F.; Dahl, K. N. Carbon Nanotubes Reorganize Actin Structures in Cells and *ex Vivo*. *ACS Nano* **2010**, *4*, 4872–4878.
30. Pampaloni, F.; Florin, E. L. Microtubule Architecture: Inspiration for Novel Carbon Nanotube-Based Biomimetic Materials. *Trends Biotechnol.* **2008**, *26*, 302–310.
31. Jordan, M. A.; Wilson, L. Microtubules and Actin Filaments: Dynamic Targets for Cancer Chemotherapy. *Curr. Opin. Cell Biol.* **1998**, *1*, 123–130.
32. Jordan, M. A.; Wilson, L. Microtubules as a Target for Anticancer Drugs. *Nat. Rev. Cancer* **2004**, *4*, 253–265.
33. (Editorial) The Dose Makes the Poison. *Nat. Nanotechnol.* **2011**, *6*, 329.
34. Piret, J. P.; Detriche, S.; Vigneron, R.; Vankoningsloo, S.; Rolin, S.; Mejia Mendoza, J. H.; Masereel, B.; Lucas, S.; Delhalle, J.; Luizi, F.; *et al.* Dispersion of Multi-Walled CNTs in Biocompatible Dispersants. *J. Nanopart. Res.* **2010**, *12*, 75–82.
35. Flahaut, E.; Laurent, Ch.; Peigney, A. Catalytic CVD Synthesis of Double and Triple-Walled Carbon Nanotubes by the Control of the Catalyst Preparation. *Carbon* **2005**, *43*, 375–383.
36. Antunes, E. F.; Lobo, A. O.; Corat, E. J.; Trava-Airoldi, V. J.; Martin, A. A.; Verissimo, C. Comparative Study of First- and Second-Order Raman Spectra of MWCNT at Visible and Infrared Laser Excitation. *Carbon* **2006**, *44*, 2202–2211.
37. Dresselhaus, S.; Dresselhaus, G.; Saito, R.; Jorio, A. Raman Spectroscopy of Carbon Nanotubes. *Phys. Rep.* **2005**, *409*, 47–99.
38. Du, J.; Ge, C.; Liu, Y.; Bai, R.; Li, D.; Yang, Y.; Liao, L.; Chen, C. The Interaction of Serum Proteins with Carbon Nanotubes Depend on the Physicochemical Properties of Nanotubes. *J. Nanosci. Nanotechnol.* **2011**, *11*, 10102–10210.
39. Ge, C.; Du, J.; Zhao, L.; Wang, L.; Liu, Y.; Li, D.; Yang, Y.; Zhou, R.; Zhao, Y.; Chai, Z.; Chen, C. Binding of Blood Proteins to Carbon Nanotubes Reduces Cytotoxicity. *Proc. Natl. Acad. Sci. U.S.A.* **2011**, *108*, 16968–16973.
40. Salvador-Morales, C.; Flahaut, E.; Sim, E.; Sloan, J.; Green, M. L.; Sim, R. B. Complement Activation and Protein Adsorption by Carbon Nanotubes. *Mol. Immunol.* **2006**, *43*, 193–201.

41. Chhikara, B. S.; Misra, S. K.; Bhattacharya, S. CNT Loading into Cationic Cholesterol Suspensions Show Improved DNA Binding and Serum Stability and Ability To Internalize into Cancer Cells. *Nanotechnology* **2012**, *23*, 065101.
42. Kaech, S.; Ludin, B.; Matus, A. Cytoskeletal Plasticity in Cells Expressing Neuronal Microtubule-Associated Proteins. *Neuron* **1996**, *17*, 1189–1199.
43. Sargent, L. M.; Hubbs, A. F.; Young, S. H.; Kashon, M. L.; Dinu, C. Z.; Salisbury, J. L.; Benkovic, S. A.; Lowry, D. T.; Murray, A. R.; Kisin, E. R.; *et al.* Single-Walled Carbon Nanotube-Induced Mitotic Disruption. *Mutat. Res.* **2012**, *14*, 28–37.
44. Wlodkowic, D.; Telford, W.; Skommer, J.; Darzynkiewicz, Z. Apoptosis and Beyond: Cytometry in Studies of Programmed Cell Death. *Methods Cell Biol.* **2011**, *103*, 55–98.
45. Lüders, J.; Stearns, T. Microtubule-Organizing Centres: A Re-evaluation. *Nat. Rev. Mol. Cell Biol.* **2007**, *8*, 161–167.
46. Shelanski, M. L.; Gaskin, F.; Cantor, C. R. Microtubule Assembly in the Absence of Added Nucleotides. *Proc. Natl. Acad. Sci. U.S.A.* **1973**, *70*, 765–768.
47. Dinu, C. Z.; Bale, S. S.; Zhu, G.; Dordick, J. S. Tubulin Encapsulation of CNTs into Functional Hybrid Assemblies. *Small* **2009**, *5*, 310–315.
48. Stepanova, T.; Slemmer, J.; Hoogenraad, C. C.; Lansbergen, G.; Dortland, B.; De Zeeuw, C. I.; Grosveld, F.; Van Cappellen, G.; Akhmanova, A.; Galjart, N. Visualization of Microtubule Growth in Cultured Neurons *via* the Use of EB1-GFP (End-Binding Protein 1-Green Fluorescent Protein). *J. Neurosci.* **2003**, *23*, 2655–2664.